An Investigation into the feasibility of Fetal Lung Maturity Prediction using Statistical Textural Features [1]

K. N. Bhanu Prakash, A. G. Ramakrishnan,

S. Suresh[*], and Teresa W P Chow[#]

Biomedical Lab., Dept. of Electrical Engg, Indian Institute of Science, Bangalore.

[*]Fetal Care Research Foundation, Madras, India.

[#]Dept of O & G, University of Malaya, Malaysia.

Short title: Fetal Lung maturity Analysis

Dr. A. G. Ramakrishnan,

Assistant Professor,

Department of Electrical Engineering,

Indian Institute of Science, Bangalore – 560 012, Karnataka, INDIA.

Email: ramkiag@ee.iisc.ernet.in

[1] Earlier brief versions of this article have appeared in [12,13].

ABSTRACT-- Fetal lung and liver tissues are examined by ultrasound in 240 subjects during 24 to 38 weeks of gestational age in order to investigate the feasibility of predicting the gestational age from the textural features of sonograms of fetal lung. A region of interest of 64 X 64 pixels is used for extracting textural features. Since the histological properties of the liver are claimed to remain constant with respect to gestational age, features obtained from the lung region are compared with those from liver. Though the means of the features show a specific trend with respect to gestation age, the variance is too high to guarantee any clustering with respect to age. Out of 64 features extracted, only 15 are unique and the rest show similar variation. A conclusion from this study is that the sonographic features, by themselves, do not unambiguously determine whether the fetal lung is mature or immature.

1. INTRODUCTION

Despite many recent advances in perinatal and neonatal care, respiratory distress syndrome (RDS) remains the major cause for morbidity and mortality. A newborn with RDS has physiologically immature lungs, which cannot support adequate gas exchange without medical intervention. Therefore, assessment of fetal lung maturity is an invaluable adjunct to modern perinatal management. RDS syndrome occurs when surface–active compounds are not present in sufficient amounts for alveoli to remain open at the end of expiration. The lung collapses and can only be opened, for further gas exchange, by the application of high positive pressure. Normal lung remains open at the end of expiration because surfactants lower surface tension on the alveolar surfaces and allow residual air to remain in the individual alveoli.

The development of fetal lung involves two components: biochemical component of fetal lung maturation is surfactant production and anatomic component is the development of airways and alveoli with fibroelastic components. Structural development of lung progresses through three stages [11]. During *glandular stage* (first 16 weeks), the lobes of the lungs become well demarcated and bronchi and bronchiole airway divisions develop. The cells lining the airways are thick and columnar proximally and change to cuboidal peripherally. During the *canalicular stage* (from 16 to 24 weeks), the development of distal airway occurs in the form of respiratory bronchiole branching and vascular proliferation at the end of airways. The cells in these distal airways change from cuboidal proximally to thinner flattened epithelial cells distally. The lungs are not yet capable of respiratory function. During the *alveolar stage* (24 weeks to term), respiratory tissue begins to appear at the ends of the respiratory bronchioles as alveolar sacs and eventually, small alveoli. During this stage, respiration can occur in a premature newborn, if surfactant production is sufficient to lower the surface tension and maintain open airspace.

Anatomic development of fetal lung seems to be closely related to gestational age (GA), while biochemical maturity can occur as early as 28 weeks or as late as term. Prediction of lung maturity is important in the management of high-risk pregnancies. If the lungs are mature to sustain the newborn with no respiratory support, then prolonging of pregnancy is not required. However, if they are immature, then the risks and costs of prolonging pregnancy may have to be weighed, especially, in settings with limited neonatal support.

Methods for determining fetal lung maturity include estimation of fetal size, gestational age, condition of placenta and biochemical tests on amniotic fluid. Though different properties of surfactants in amniotic fluid have been studied, the Lecithin/Sphingomyelin ratio (L/S ratio) remains the golden standard. All these tests necessitate amniocentesis, an invasive procedure that carries risks, and on occasion, may be contraindicated. Ultrasound can neither measure any of the biochemical parameters of fetal lung maturity nor can it provide direct histological information about fetal lung development. However, experimental evidences support the hypothesis that morphological and biochemical changes alter the diffuse scattering and other propagation properties of fetal lung. Such a change translates to appropriate variations in the textural appearance of sonogram. Sonographically determined parameters such as fetal biparietal diameter and placental grading have been related to fetal maturity, with accuracy ranging from 78% to 100% [5].

Arguments for and against the use of sonographic features for analyzing fetal lung maturity have been extensively debated [1,2,3,4,5]. Based on sonographic studies, Thieme *et al*. [1] conclude that the reflectivity of lung is greater than liver reflectivity during mid – gestation and is equal to liver reflectivity at term in lamb. Garrett *et al.*[2] In 1980 stated that reflectivity of the human fetal lung is equal to or less than that of liver throughout most of pregnancy but

that relationship reverses in late gestation. Nevertheless, Cayea *et al.* [3] argue that there is no statistically significant correlation between the sonographic features and the biochemical fetal lung maturity indices, namely L/S ratio and Phosphatidylglycerol (PG) values. Employing RF signals for characterizing fetal lung and liver tissues, Benson *et al.* [4] observe, from the reflected signals, a spectral shift from a higher frequency range to a lower frequency range as the fetal lung makes the transition from immature to mature state. Feingold *et al.* [5] use densitometer measurements to establish a correlation between lung–liver echogenicity and the L/S ratio. Podobnik *et al.* [6] bring forth a relation between the coefficient of variation of lung-liver echogenicity and the L/S ratio. In the present study, our motivation is to explore the possibility of estimating the gestation age using the textural features of the sonogram. The investigation involves a computational analysis of the various textural features of the sonogram and their dynamics with lung maturity.

2. MATERIALS AND METHODS

Ultrasound examinations were performed using the real time ATL Apogee 800 plus scanner with a 3.5 MHz curvilinear, broad bandwidth transducer probe with the dynamic range set at 55 dB. The overall gain was set at an optimal value to get uniform visibility. The appropriate section was frozen and the image was grabbed. Longitudinal and transverse sections of the fetal thorax and upper abdomen were imaged. The fetal lung and liver were identified in the thoracic and upper abdominal sections respectively. Care was taken to avoid obvious vascular structures in the liver. Data was collected from 240 subjects in regular intervals at various gestation ages from 24 to 38 weeks. Data was collected both at Mediscan Systems, Chennai, India and at the University Hospital in Kuala Lumpur, Malaysia. The images were

frozen in the machine and then transferred to a video tape. The images were then digitized using the Creative video grabber card. The size of the digitized image is 320 X 240 pixels with a resolution of 29 pixels per centimeter. The images were normalized to have the same range of gray values by the histogram equalization technique. A region of interest of 64 X 64 pixels was used for extracting a number of quantitative parameters related to texture. The lung to liver ratios of various feature values were studied as possible indices of maturity. The details of the features employed are given below.

2.1 Spatial Gray Level Dependence Matrices (SGLDM)

The SGLDM are based on the estimation of second order joint conditional probability density functions, $f(i, j| d, \theta)$. Here $f(i, j| d, \theta)$ is the probability that a pair of pixels separated by a distance d at an angle θ have gray levels i and j. The angles are quantized to 45^0 intervals. The estimated probability density functions, denoted by,

$P(i, j| d, \theta)$ are defined as,

$$P(i,j \mid d,0) = \#\{((k,l),(m,n)) \in (L_X \times L_Y) \times (L_Y \times L_X) : k = m, |l - n| = d, I(k, l) = i, I(m,n) = j\} / T(d,0)$$

$$P(i,j \mid d,45^0) = \#\{((k,l),(m,n)) \in (L_X \times L_Y) \times (L_Y \times L_X) : (k - m = d, l - n = -d) \text{ or } (k - m = -d, l-n = d), I(k, l) = i, I(m,n) = j\} / T(d,45^0)$$

$$P(i,j \mid d,90^0) = \#\{((k,l),(m,n)) \in (L_X \times L_Y) \times (L_Y \times L_X) : |k - m| = d, l = n, I(k, l) = i, I(m,n) = j\} / T(d,90^0)$$

$$P(i,j \mid d,135^0) = \#\{((k,l),(m,n)) \in (L_X \times L_Y) \times (L_Y \times L_X) : (k - m = -d,\ l - n = -d,\ I(k,l) = i,\ I(m,n) = j\} / T(d,135^0)$$

where # denotes the number of elements in the set, L_X and L_Y are the horizontal and vertical spatial domains, $I(x, y)$ is the image intensity at point (x,y), $T(d, \theta)$ stands for the total number of pixel pairs within the image which have the inter-sample spacing d and direction angle θ. If a texture is coarse and d is small compared to the sizes of the texture elements, the pairs of points at separation distance d should usually have similar gray values. Conversely, for fine structures the gray levels of points separated by distance d should often be quite different.

Haralick [7] proposed 14 texture measures that can be extracted from the $P(i,j \mid d,\theta)$ matrices. In our study, only the following five texture features [8] are computed.

$$\text{Energy: } E(S_\theta(d)) = \sum_{i=0}^{N_G-1}\sum_{j=0}^{N_G-1}[s_\theta(i,j \mid d)]^2$$

$$\text{Entropy: } H(S_\theta(d)) = -\sum_{i=0}^{N_G-1}\sum_{j=0}^{N_G-1}s_\theta(i,j \mid d)\log s_\theta(i,j \mid d)$$

$$\text{Correlation: } C(S_\theta(d)) = \frac{\sum_{i=0}^{N_G-1}\sum_{j=0}^{N_G-1}(i-\mu_x)(j-\mu_y)s_\theta(i,j \mid d)}{\sigma_x\sigma_y}$$

$$\text{Inertia: } (S_\theta(d)) = \sum_{i=0}^{N_G-1}\sum_{j=0}^{N_G-1}(i-j)^2 s_\theta(i,j \mid d)$$

$$\text{Local Homogeneity: } L(S_\theta(d)) = \sum_{i=0}^{N_G-1}\sum_{j=0}^{N_G-1}\frac{1}{1+(i-j)^2}s_\theta(i,j \mid d)$$

where $s_\theta(i, j \mid d)$ is the $(i,j)^{\text{th}}$ element of S_θ for a specified d, N_G is the number of gray levels in the image and

$S_0(d) = P(i, j \mid d, 0^0)$; $S_{45}(d) = P(i, j \mid d, 45^0)$;

$S_{90}(d) = P(i, j \mid d, 90^0)$; and $S_{135}(d) = P(i, j \mid d, 135^0)$;

$$\mu_x = \sum_{i=0}^{N_G-1} i \sum_{j=0}^{N_G-1} s_\theta(i, j \mid d) \qquad \mu_y = \sum_{j=0}^{N_G-1} j \sum_{i=0}^{N_G-1} s_\theta(i, j \mid d)$$

$$\sigma^2{}_x = \sum_{i=0}^{N_G-1} (i - \mu_x)^2 \sum_{j=0}^{N_G-1} [s_\theta(i, j \mid d)] \qquad \sigma^2{}_y = \sum_{j=0}^{N_G-1} (j - \mu_y)^2 \sum_{i=0}^{N_G-1} [s_\theta(i, j \mid d)]$$

Each measure is evaluated for d=1 and $\theta = 0^0, 45^0, 90^0$ and 135^0.

2.2 The Gray Level Difference Matrix (GLDM)

For any given displacement $\delta = (\Delta x, \Delta y)$, let $I_\delta(x, y) = |I(x, y) - I(x+\Delta x, y+ \Delta y)|$ and $f'(i \mid \delta)$ be the probability density of $I_\delta(x, y)$. If there are m gray values, this has the form of a m-dimensional vector whose i^{th} component is the probability that $I_\delta(x, y)$ will have value i. The value of $f'(i \mid \delta)$ is obtained from the number of times $I_\delta(x, y)$ occurs for a given δ. Explicitly,

$$f'(i \mid \delta) = P(I_\delta(x, y) = i)$$

Four possible forms of the vector δ are considered: (0,d), (-d, d), (d, 0), and (-d, -d), where d is the inter-pixel distance. From each of these density functions, five texture features were extracted. They are:

Contrast: $CON = \sum_{i=0}^{N_G-1} i^2 f'(i \mid \delta)$

$Mean = \sum_{i=0}^{N_G-1} i f'(i \mid \delta)$

Entropy: $ENT = \sum_{i=0}^{N_G-1} f'(i \mid \delta) \log(f'(i \mid \delta))$

Inverse Difference Moment: $IDM = \sum_{i=0}^{N_G-1} \frac{f'(i \mid \delta)}{i^2 + 1}$

Angular Second Moment: $ASM = \sum_{i=0}^{N_G-1} [f'(i \mid \delta)]^2$

2.3 Laws' Texture Energy Measures

Laws' texture energy measures [9] are derived from three vectors, each of length three: ***L3 = (1, 2, 1), E3 = (-1, 0, 1) and S3 = (-1, 2, -1)***. These, respectively, represent the operations of local averaging, edge detection and spot detection. If these vectors are convolved with themselves or with one another, we obtain, among others, the following five vectors, each of length five: ***L5 = (1, 4, 6, 4, 1), S5 = (-1, 0, 2, 0, -1), R5 = (1, -4, 6, -4, 1), E5 = (-1, -2, 0, 2, 1)*** and ***W5=(-1, 2, 0, -2, 1)*** which perform local averaging, spot, ripple, edge and wave detection, respectively. The masks used in our analysis are

$L5^T E5$					$L5^T S5$.				
-1	**-2**	**0**	**2**	**1**	**-1**	**0**	**2**	**0**	**-1**
-4	**-8**	**0**	**8**	**4**	**-4**	**0**	**8**	**0**	**-4**
-6	**-12**	**0**	**12**	**6**	**-6**	**0**	**12**	**0**	**-6**
-4	**-8**	**0**	**8**	**4**	**-4**	**0**	**8**	**0**	**-4**
-1	**-2**	**0**	**2**	**1**	**-1**	**0**	**2**	**0**	**-1**

The masks were convolved with the image and the entropy of the resulting image was calculated.

2.4. Fractal dimension and Lacunarity

The above conventional methods measure the coarseness, directionality and energy. However, they do not consider an important characteristic, namely, the granularity. An intensity surface of an ultrasonic image can be viewed as the end result of random walks and a fractional Brownian motion model [10] can be used for its analysis. Fractal dimension and lacunarity are the important features that characterize the roughness and granularity of the fractal surface.

Given a $M \; X \; M$ image I, the intensity difference vector is defined as $IDV = [id(1), \; id(2),... \; id(s)]$, where s is the maximum possible scale and $id(k)$ is the average of the absolute intensity difference of all pixel pairs with horizontal or vertical distance k. We compute $id(k)$ as

$$id(k) = \frac{\sum_{x=0}^{M-1}\sum_{y=0}^{M-k-1} |I(x,y) - I(x,y+k)| + \sum_{x=0}^{M-k-1}\sum_{y-0}^{M-1} |I(x,y) - I(x+k,y)|}{2M(M-k-1)}$$

and $D = 3 - H$, where D is the fractal dimension. The value of H is obtained by using least-squares linear regression to estimate the slope of the curve of $id(k)$ versus k in log-log scale. Given a fractal set A, let $P(m)$ be the probability that there are m points within a box of size L, centered about an arbitrary point of A. We have $\sum_{m=1}^{N} P(m) = 1$, where N is the number of possible points within the box. Lacunarity is, then, defined as

$$\Lambda = \frac{(M_2 - M^2)}{M^2},$$

where $M = \sum_{m=1}^{N} mP(m)$ and $M_2 = \sum_{m=1}^{N} m^2 P(m)$

3. RESULTS AND DISCUSSION

Out of the 64 features extracted, only 15 features are found to be unique and the rest are redundant. Since the features of GLDM and SGLDM have similar variations, and further since computation of SGLDM features is both time and memory consuming, we discard the SGLDM features. The features selected are: (i) fractal dimension, (ii) intercept from fractal measures, (iii) lacunarity from fractal measures, (iv) contrast, (v) angular second moment, (vi) entropy, (vii) mean from GLDM, (viii) inverse difference moment from GLDM, (ix) entropy measures from the $\boldsymbol{L5^T E5}$ mask, (x) entropy measures from the $\boldsymbol{L5^T S5}$ mask, (xi) mean from the histogram of the image, (xii) variance from the histogram, (xiii) coefficient of variation from the histogram, (xiv) skewness of the histogram, and (xv) kurtosis of the histogram. It is observed that data sets from both the hospitals exhibit similar behavior. Figure 1 illustrates the variation with respect to the gestation age of the mean (for all the subjects) of the ratios of the value of lung to liver feature. This variation has been presented for all the above 15 features. We can see that only four of the parameters, namely, fractal dimension, lacunarity from fractal measures, variance from the histogram, and coefficient of variation from the histogram have some trend that could possibly have some predictive value. However, the coefficient of variation depends on the variance, and as seen from the figure, has almost identical variations as that of the latter, and thus does not contribute any new information.

Figure 2 demonstrates the dynamics of the chosen features as a function of the gestation age for the lung and the liver. As seen from the figure, the nature of variation of the features of

the liver is, in most cases, similar to that of the lung. Since the tissues imaged are at the same depth for both the lung and the liver, the features, which are mainly textural in nature, are reasonably insensitive to the settings of the imaging system. This questions one of the basic assumptions, namely, that the sonographic features of the liver are expected to remain constant, starting from the gestation age of 24 weeks, and thus can be taken as a reference. The conclusions of most of the previous investigators are based on the study of only the echogenicity of the liver and lung, which are sensitive to the imaging parameters.

Figure 3 displays the variation of the mean ratio of lung-liver features with respect to gestation age, with a confidence level of 0.99. It also identifies the feature points that lie outside the confidence interval.

Figure 4 shows the box-plots of the features with their mean and variance. It also gives the information on the number of outliers in each group. Out of the 15 features selected, only 6 features are found to be exhibiting notable dynamics as a function of the gestation age. They are fractal dimension, lacunarity, differential contrast, mean, variance and coefficient of variation. It is observed from Fig. 4A that, around the time when the lung tissue is supposed to be fully mature (36 weeks), there is a sudden increase of the outliers for the fractal dimension. This anomalous behavior of the ratio of the fractal dimensions of lung to the liver may be a characteristic of the transition from immaturity to maturity of the lung. An analysis of data from high risk pregnancies (hypertensive mothers) could confirm whether this is an expected trend in all cases of maturity. Figure 5 illustrates that all the feature values are nearly normally distributed at each gestation age. Figure 6 exhibits samples of the liver and lung image files for each gestation age.

The cells of the lung are found elongated during early gestation period. This could give rise to images that are quite smooth and less granular in nature. The cells become cuboidal towards the term resulting in more granular images. Due to this change in granularity, we expect an increase in the fractal dimension and lacunarity of the images. The graphs show a trend similar to what is expected. The mean graph shows a decrease in the echogenicity of lung as compared to the liver as the gestation age increases. The echogenicity of the lung is almost the same as the echogenicity of the liver at early gestation age. Thus, the lung seems to attenuate ultrasound waves more than the liver at later gestation ages (cf. [4]). The variance of the gray values of the lung has an upward trend whereas that of the liver remains almost at the same level.

4. CONCLUSIONS

The ultrasound image formation depends on many factors. Though we have tried to maintain most of the parameters at a constant value, it is not possible to have fixed settings of the parameters of the ultrasound machine because the subjects are of different obesity and also have different attenuation levels. Further, the position of the baby in certain cases may not yield good view field. However, since in all the cases, the lung and the liver have been imaged together, the effects due to the imaging techniques (including the internal processing by the machine) must affect both the regions identically, and thus must not cause any variations on the textural features of the lung and liver differentially. Thus the textural features are better indicators of the histological changes, compared to the study of only the echogenicity. Based on the data analyzed, it appears that an unambiguous decision, about the maturity of the fetal lung, cannot be made purely based on the characteristics of the ultrasound images. However, some of the features studied show some notable trend. Thus, a complete sonographic analysis, which

combines the above textural features with parameters such as fetal biparietal diameter, placental grading, femur length, head circumference and the abdominal circumference could possibly enhance the prediction accuracy.

BIBLIOGRAPHY

[1] THIEME, G. A., BANJAVIC, R. A., JOHNSON, M. L., MEYER, C. R., SILVERS, G. W., HERRON, D. S., AND CARSON. “Sonographic identification of lung maturation in the fetal lamb,” *Invest. Radiology*, 1983; vol. 18, page18 -26.

[2] GARRETT, W. J., WARREN, P. S., AND PICKER, R. H., “Maturation of the fetal lung, liver, and bowel,” *Proc. Am. Inst. Ultras. Med.,* 1980, 93 (abstr).

[3] CAYEA P. D., GRANT D.C., DOUBILET P.M., AND JONES.T.B “Prediction of fetal lung maturity: inaccuracy of study using conventional ultrasound instruments,” *Radiology*, 1985; vol. 155, page 473--475.

[4] D. M. BENSON AND L. D. WALDROUP “Ultrasonic tissue characterization of fetal lung, liver and placenta for the purpose of assessing fetal maturity,” *Journal of Ultrasound in Medicine*, 1983; vol. 2, page 489--494.

[5] MICHAEL FEINGOLD, JAMES SCOLLINS, CURTIS CETRULO, AND DOGLAS KOZA. “Fetal lung to liver reflectivity ratio and lung maturity,” *Journal of Clinical Ultrasound*, 1987; vol. 15, page 384--387.

[6] M. PODOBNIK, B. BRAYER, AND B. CIGLAR. “Ultrasonic fetal and placenta tissue characterization and lung maturity,” *International Journal of Gynecology and Obstetrics*, 1996; vol. 54: page 221--229.

[7] RM HARALICK “Statistical and structural approaches to texture,” *Proc. IEEE*, 1979, vol. 67(5), p. 304-322.

[8] R. W. CONNERS AND C. A. HARLOW “A theoretical comparison of texture algorithms,” *IEEE Trans. PAMI*, 1980; vol. 2(3): p. 204--222.

[9] K. I. LAWS. “Texture energy measures,” *Proc. Image understanding Workshop*, 1979; pages 47--51.

[10] KELLER, J. M., CHEN, S., AND CROWNOVER. “Texture description and segmentation through fractal geometry,” *Computer Vision, Graphics and Image Processing*, 1989; vol. 45: page 150--166.

[11] CHARNOCK, E.L. AND DOERSHUK, C.F., “Developmental aspects of the human lung,” *Pediatr. Clin. North America., 20, 275-292, 1973.*

[12] K.N.BHANU PRAKASH, S. SURESH AND A.G. RAMAKRISHNAN, “Can Sonogram predict fetal lung maturity?,” *Critical Reviews in Biomedical Engineering*, Vol. 26, Issues 5 & 6, 1998, page 350-351.

[13] K.N.BHANU PRAKASH, A.G.RAMAKRISHNAN, S.SURESH AND TERESA W P CHOW, “Fetal lung maturity analysis using sonogram textural features,” *Proc. Symposium on Biomedical Engineering –2000*, BARC, Mumbai, India, Jan.2000, pp. 155 –158.

FIGURE CAPTIONS

1. Plot showing the variation of means of the ratios of lung to liver feature values with respect to the gestation age. Top Row (L - R): Fractal Dimension, Intercept, Lacunarity, Contrast calculated from GLDM; Second Row (L - R): Angular Second Moment, Entropy from GLDM, Mean from GLDM, Inverse difference moment; Third row (L – R): Entropy after applying the Laws mask $L5^T$ E5, Entropy after the mask $L5^T$S5, Mean calculated from the histogram of the image, Variance obtained from the histogram; Bottom Row (L – R) : Coefficient of Variation, Skewness calculated from the histogram, Kurtosis computed from the histogram.

2. Plot showing the variation of the mean of various features of lung (—) and liver (----) with respect to the gestation age. Top Row (L - R): Fractal Dimension, Intercept, Lacunarity, Contrast calculated from GLDM; Second Row (L - R): Angular Second Moment, Entropy from GLDM, Mean from GLDM, Inverse difference moment; Third row (L – R): Entropy after applying Laws textural mask $L5^t$ E5, Entropy after the mask $L5^T$S5, Mean calculated from the histogram of the image, Variance obtained from the histogram; Bottom Row (L – R) : Coefficient of Variation, Skewness computed from the histogram, Kurtosis calculated from the histogram.

3. Xbarplots showing the variation of selected features with respect to gestation age.

Page – 23 : Top Row :- A: Fractal Dimension ;

B: Intercept ;

Bottom Row :- C: Lacunarity ;

D: Contrast ;

Page –24: Top Row :- E : Angular Second Moment;

F: Entropy ;

Bottom Row :- G: Mean calculated from GLDM ;

H: Inverse difference moment ;

Page – 25 : Top Row :- I : Entropy calculated after application of Laws textural mask $L5^{T}E5$;

J : Entropy calculated after application of mask $L5^{T}S5$;

Bottom Row :-K : Mean calculated from histogram of the image ;

L : Variance calculated from the histogram;

Page –26 : Top Row:- M : Coefficient of Variation;

N : Skewness calculated from the histogram;

Bottom Row :- O : Kurtosis calculated from the histogram.

4. Boxplots showing the variation of selected features with respect to gestation age.

Page – 27 : Top Row :- A: Fractal Dimension ;

B: Intercept ;

Bottom Row :- C: Lacunarity ;

D: Contrast ;

Page –28: Top Row :- E : Angular Second Moment;

F: Entropy ;

Bottom Row :- G: Mean calculated from GLDM ;

H: Inverse difference moment ;

Page – 29 : Top Row :- I : Entropy calculated after application of Laws textural mask $L5^{T}E5$;

J : Entropy calculated after application of mask $L5^{T}S5$;

Bottom Row :-K : Mean calculated from histogram of the image ;

L : Variance calculated from the histogram;

Page –30 : Top Row:- M : Coefficient of Variation;

N : Skewness calculated from the histogram;

Bottom Row :- O : Kurtosis calculated from the histogram.

5. Plots showing that each feature value at each gestation age is normally distributed.

Page 31 : Fractal Dimension, Top Row (L-R) Gestation age 24, 26 and 28 weeks

Middle Row (L-R) Gestation age 30,32 and 34 weeks

Bottom Row (L-R) Gestation age 36 and 38 weeks

Page 32 : Lacunarity, Top Row (L-R) Gestation age 24, 26 and 28 weeks

Middle Row (L-R) Gestation age 30,32 and 34 weeks

Bottom Row (L-R) Gestation age 36 and 38 weeks

Page 33 : Contrast calculated Top Row (L-R) Gestation age 24, 26 and 28 weeks

from GLDM Middle Row (L-R) Gestation age 30,32 and 34 weeks

Bottom Row (L-R) Gestation age 36 and 38 weeks

Page 34 : Mean calculated Top Row (L-R) Gestation age 24, 26 and 28 weeks

from histogram Middle Row (L-R) Gestation age 30,32 and 34 weeks

Bottom Row (L-R) Gestation age 36 and 38 weeks

Page 35: Variance calculated Top Row (L-R) Gestation age 24, 26 and 28 weeks

from histogram Middle Row (L-R) Gestation age 30,32 and 34 weeks

Bottom Row (L-R) Gestation age 36 and 38 weeks

Page 36 : Coefficient of variation calculated from histogram

Top Row (L-R) Gestation age 24, 26 and 28 weeks

Middle Row (L-R) Gestation age 30,32 and 34 weeks

Bottom Row (L-R) Gestation age 36 and 38 weeks

6. Sample Images for each gestational age.

Top Row : Liver Images at 24 26 28 & 30 weeks

Second Row : Liver Images at 32 34 36 & 38 weeks

Third Row : Lung Images at 24 26 28 & 30 weeks

Bottom Row : Lung Images at 32 34 36 & 38 weeks

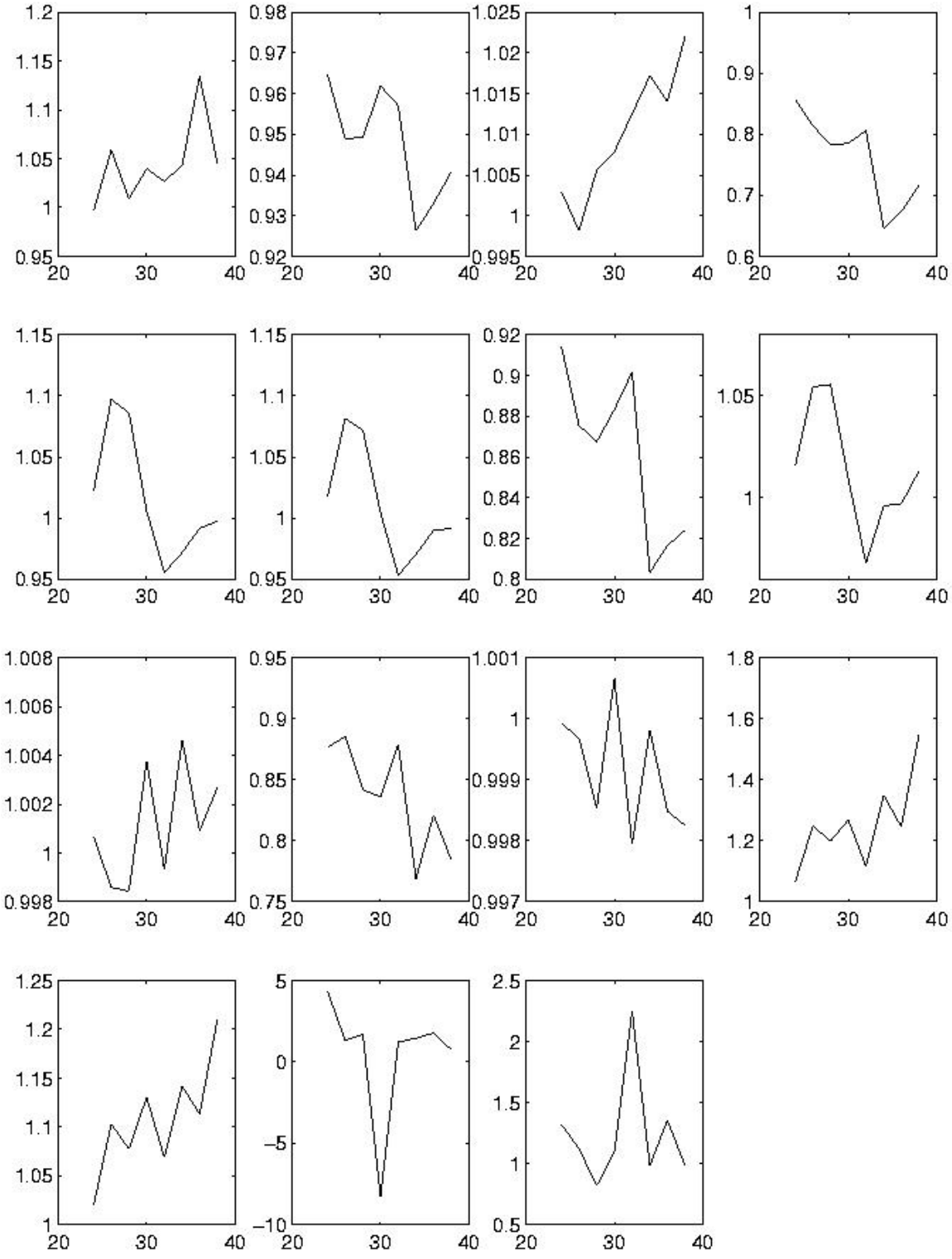
1.2
1.15
1.1
1.05
1
0.95
20
30
40
0.98
0.97
0.96
0.95
0.94
0.93
0.92
1.025
1.02
1.015
1.01
1.005
1
0.995
1
0.9
0.8
0.7
0.6
1.15
1.1
1.05
0.92
0.9
0.88
0.86
0.84
0.82
0.8
1.008
1.006
1.004
1.002
0.998
0.95
0.85
0.75
1.001
0.999
0.998
0.997
1.8
1.6
1.4
1.2
1.25
5
0
−5
−10
2.5
2
1.5
0.5

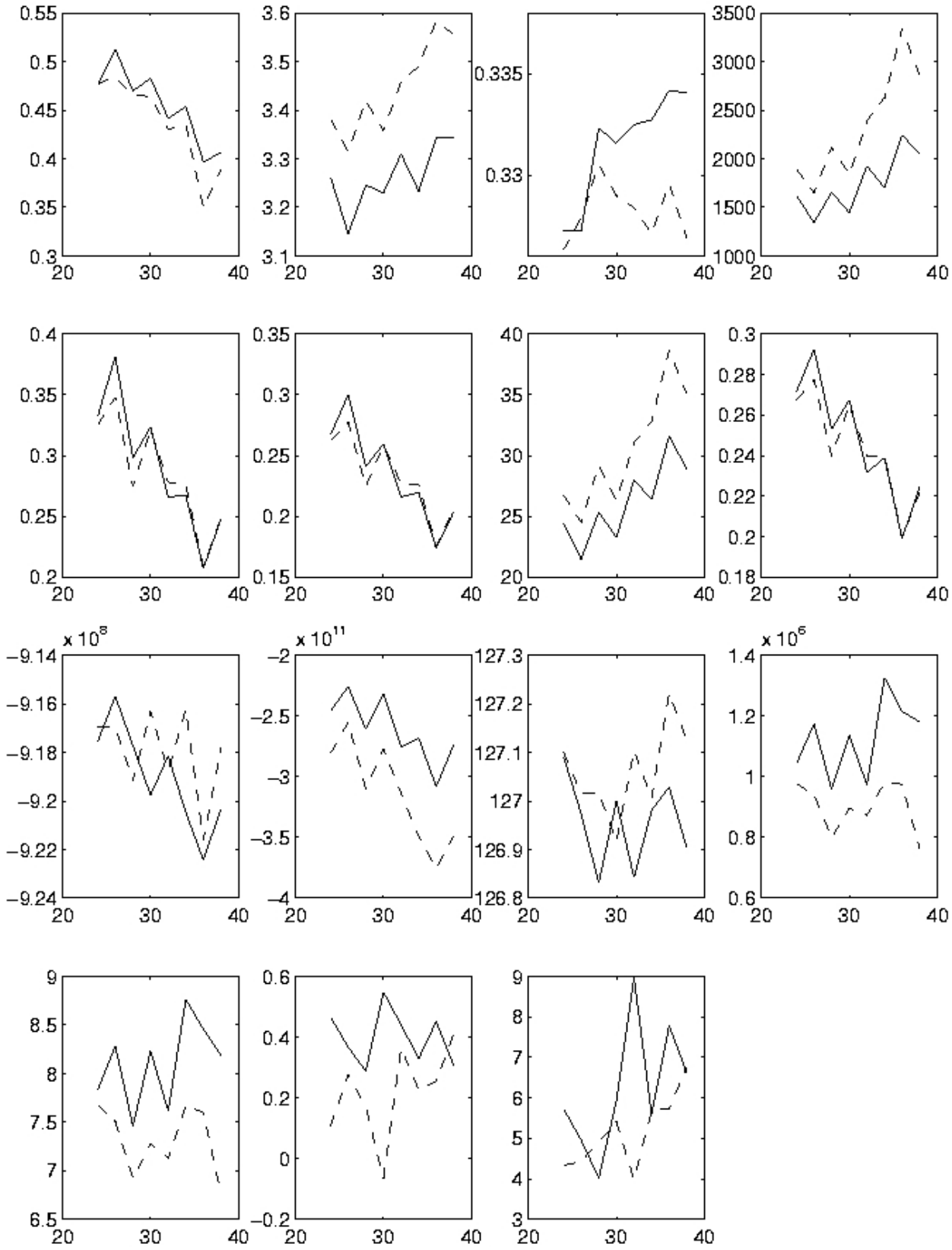
0.55
0.5
0.45
0.4
0.35
0.3
20
30
40
3.6
3.5
3.4
3.3
3.2
3.1
0.335
0.33
3500
3000
2500
2000
1500
1000
0.4
0.35
0.3
0.25
0.2
0.15
40
35
30
25
20
0.3
0.28
0.26
0.24
0.22
0.2
0.18
x 10^8
−9.14
−9.16
−9.18
−9.2
−9.22
−9.24
x 10^11
−2
−2.5
−3
−3.5
−4
127.3
127.2
127.1
127
126.9
126.8
x 10^5
1.4
1.2
1
0.8
0.6
9
8.5
8
7.5
7
6.5
0.6
0.4
0.2
0
−0.2
9
8
7
6
5
4
3

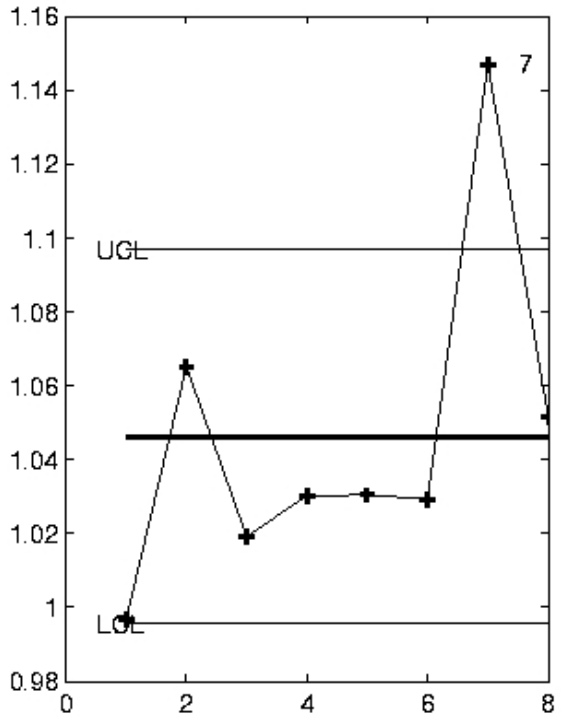
1.16
1.14
1.12
1.1
1.08
1.06
1.04
1.02
1
0.98
UCL
LCL
7
0
2
4
6
8

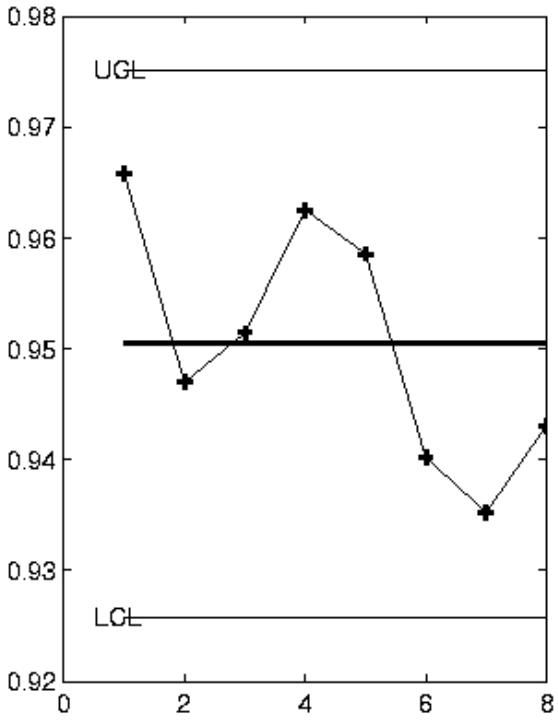
0.98
0.97
0.96
0.95
0.94
0.93
0.92
UCL
LCL
0
2
4
6
8

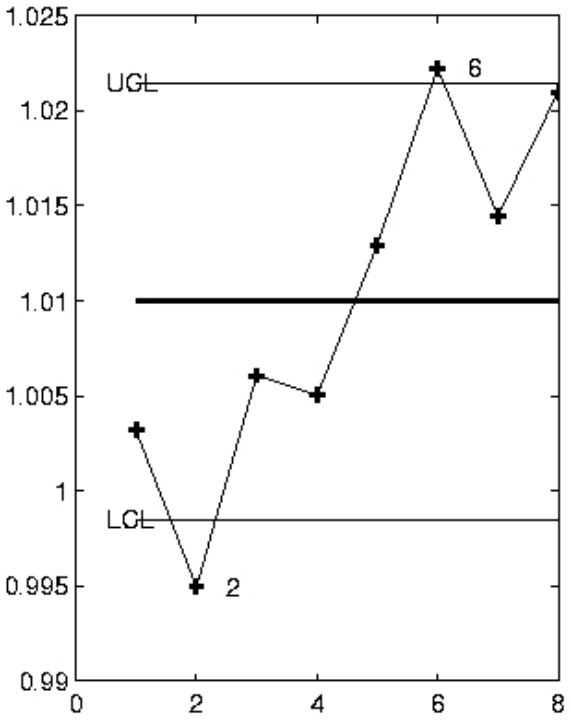
1.025
1.02
1.015
1.01
1.005
1
0.995
0.99
UCL
LCL
6
2
0
2
4
6
8

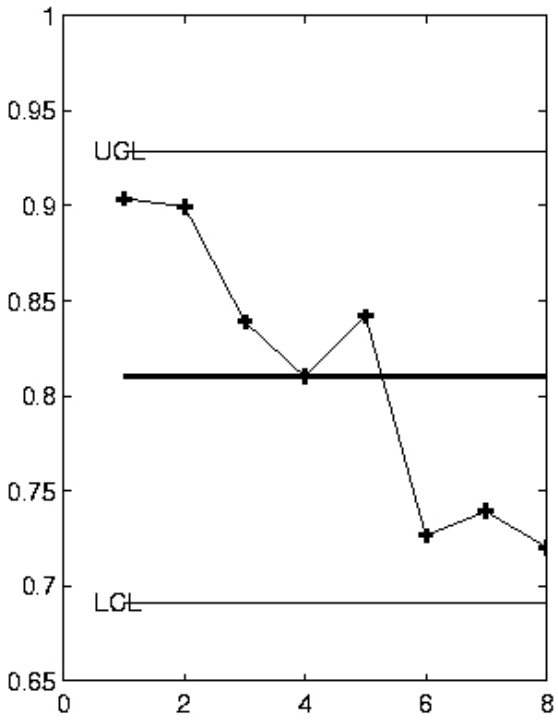
1
0.95
0.9
0.85
0.8
0.75
0.7
0.65
UCL
LCL
0
2
4
6
8

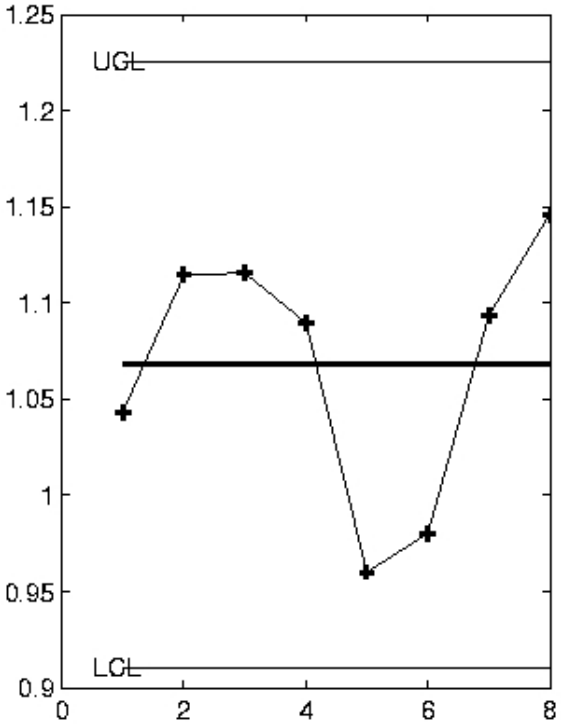
UCL
LCL
1.25
1.2
1.15
1.1
1.05
1
0.95
0.9
0
2
4
6
8

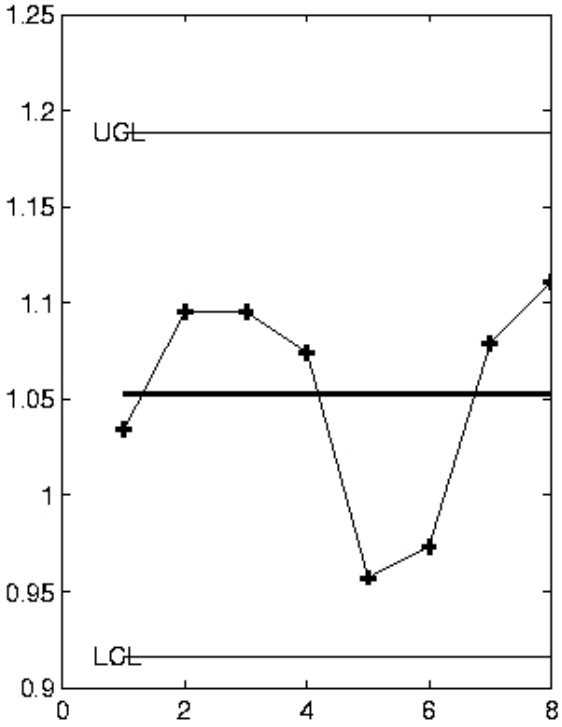
UCL
LCL
1.25
1.2
1.15
1.1
1.05
1
0.95
0.9
0
2
4
6
8

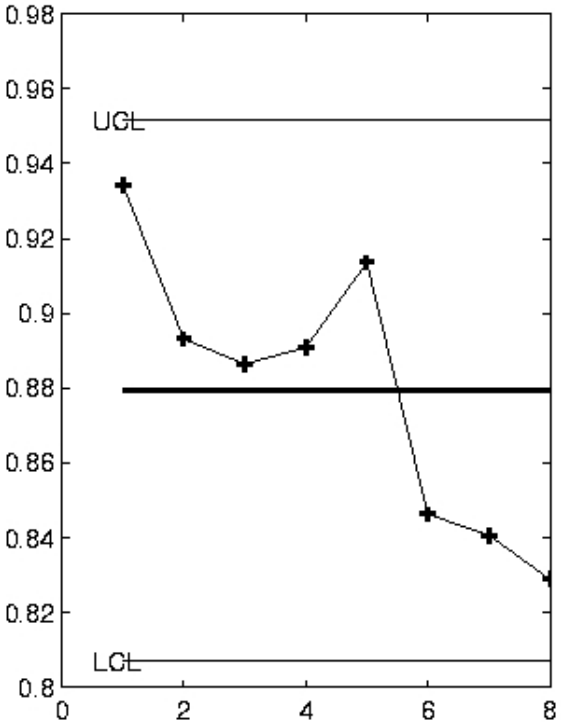
UCL
LCL
0.98
0.96
0.94
0.92
0.9
0.88
0.86
0.84
0.82
0.8
0
2
4
6
8

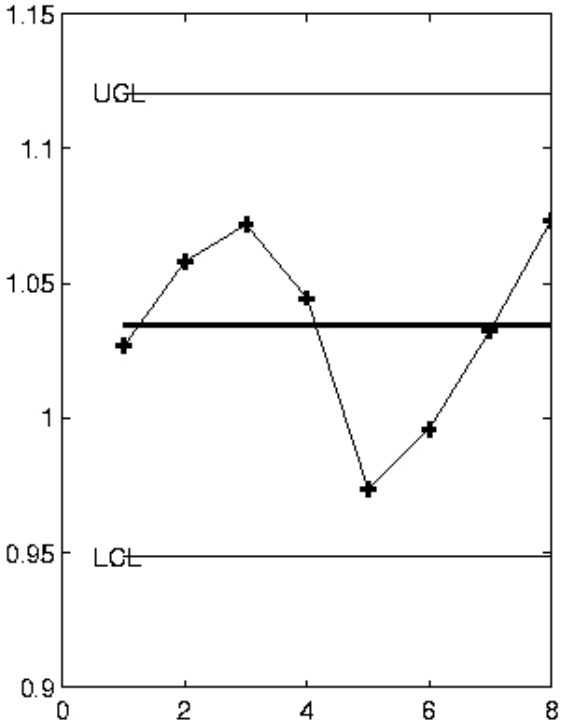
UCL
LCL
1.15
1.1
1.05
1
0.95
0.9
0
2
4
6
8

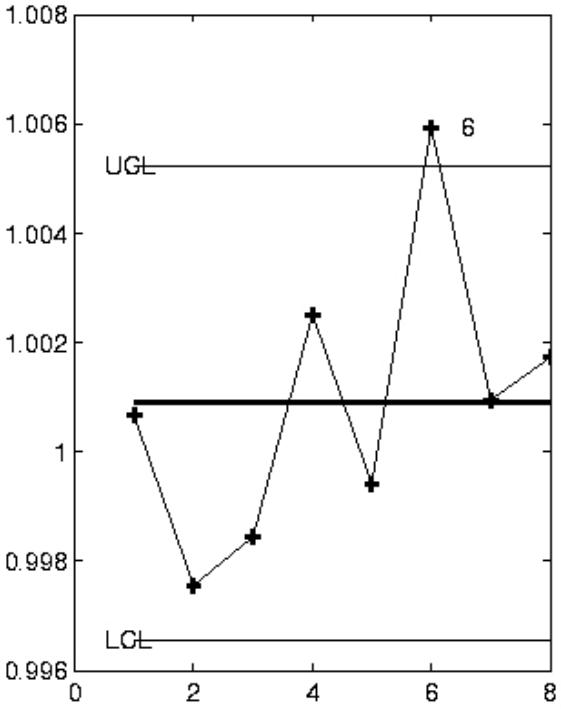
1.008
1.006
1.004
1.002
1
0.998
0.996
0
2
4
6
8
6
UCL
LCL

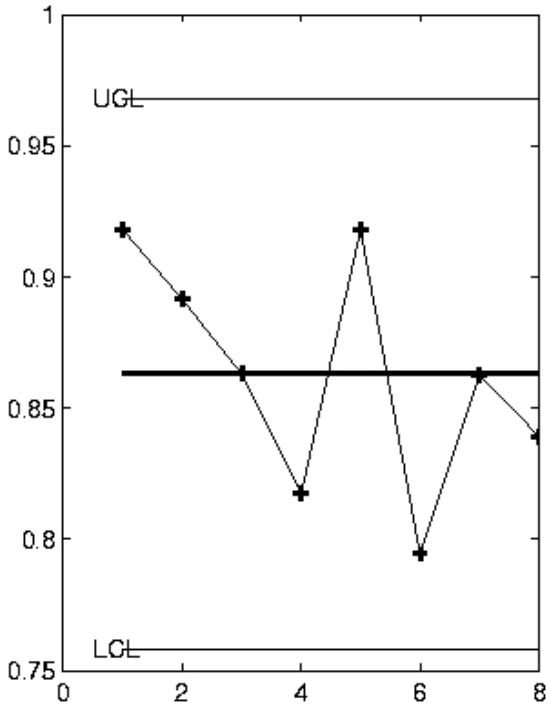
1
0.95
0.9
0.85
0.8
0.75
0
2
4
6
8
UCL
LCL

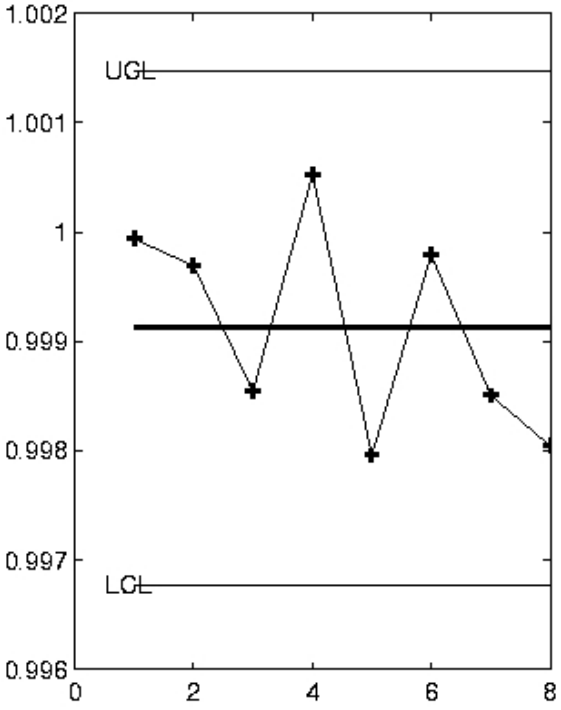
1.002
1.001
1
0.999
0.998
0.997
0.996
0
2
4
6
8
UCL
LCL

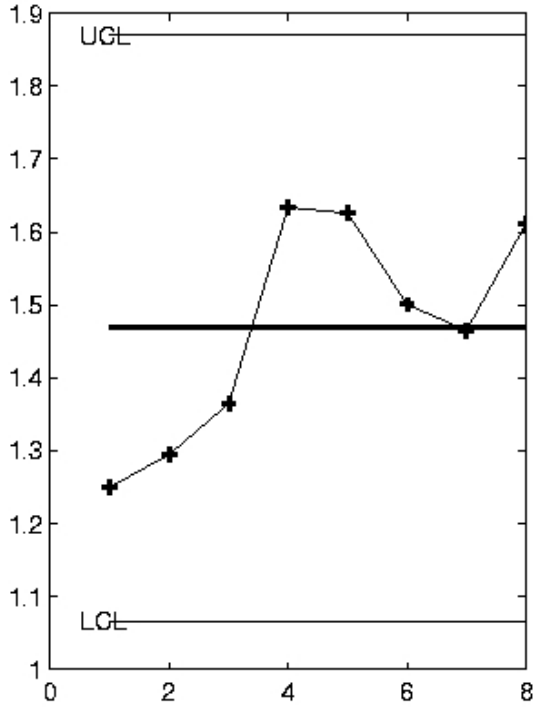
1.9
1.8
1.7
1.6
1.5
1.4
1.3
1.2
1.1
1
0
2
4
6
8
UCL
LCL

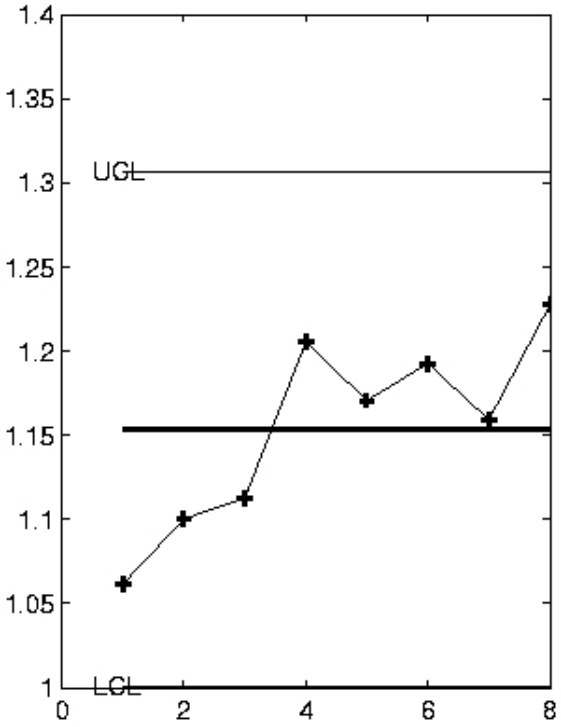
UCL
LCL

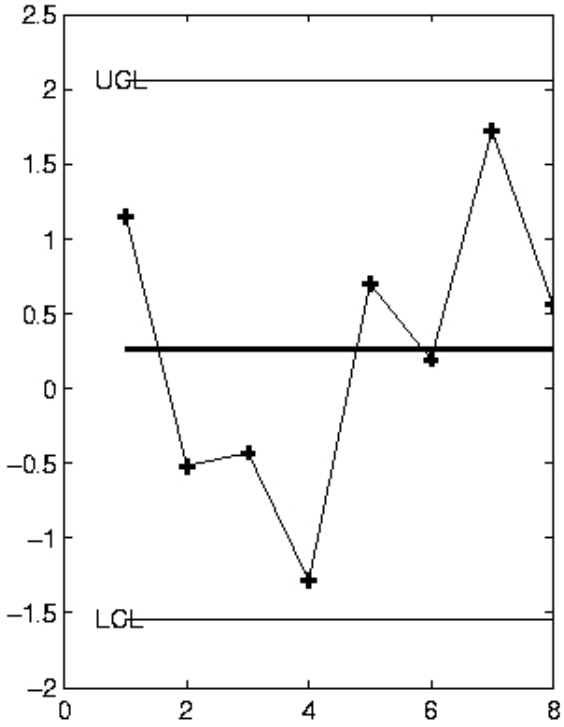
UCL
LCL

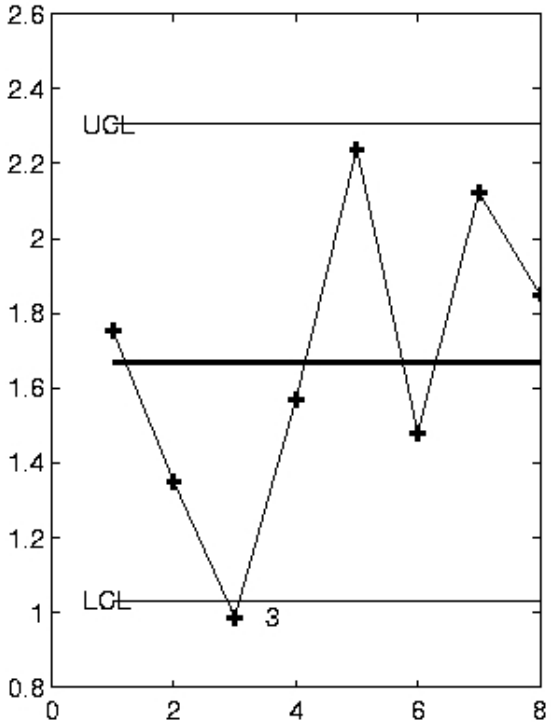
UCL
LCL
3

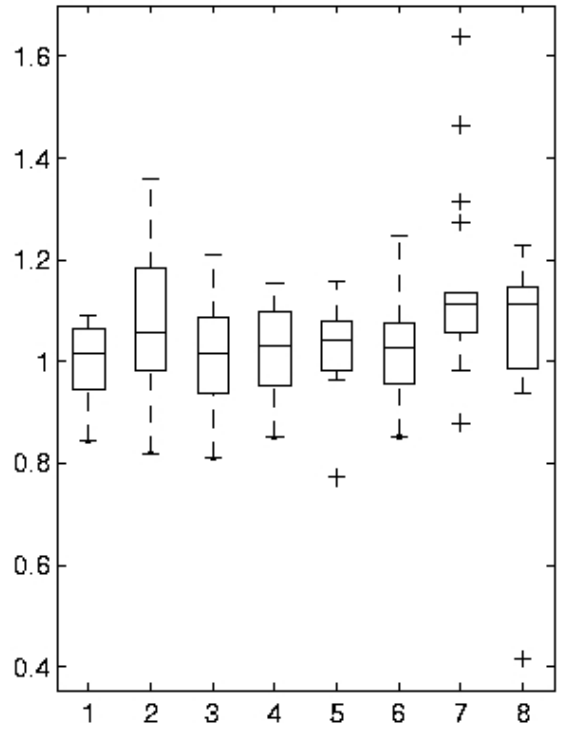
1.6
1.4
1.2
1
0.8
0.6
0.4
1 2 3 4 5 6 7 8

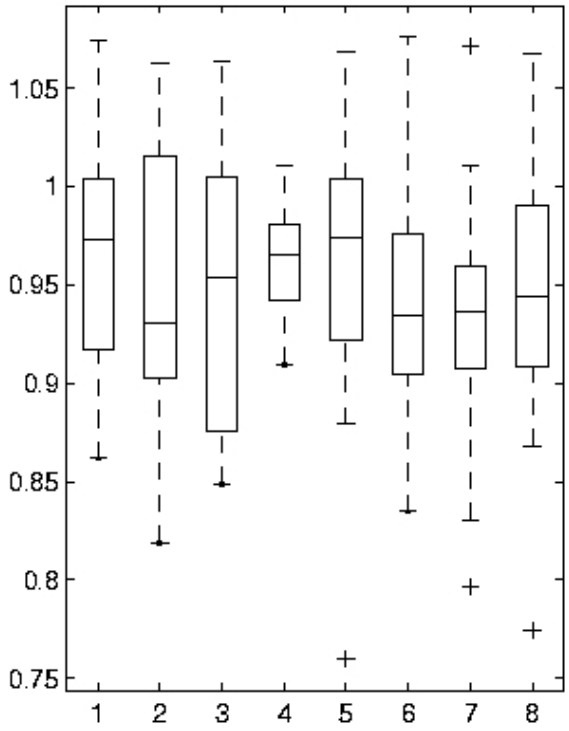
1.05
1
0.95
0.9
0.85
0.8
0.75
1 2 3 4 5 6 7 8

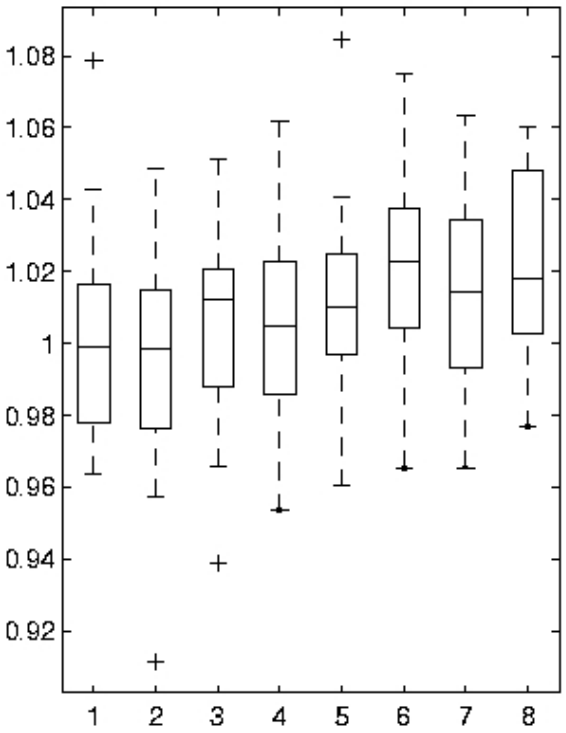
1.08
1.06
1.04
1.02
1
0.98
0.96
0.94
0.92
1 2 3 4 5 6 7 8

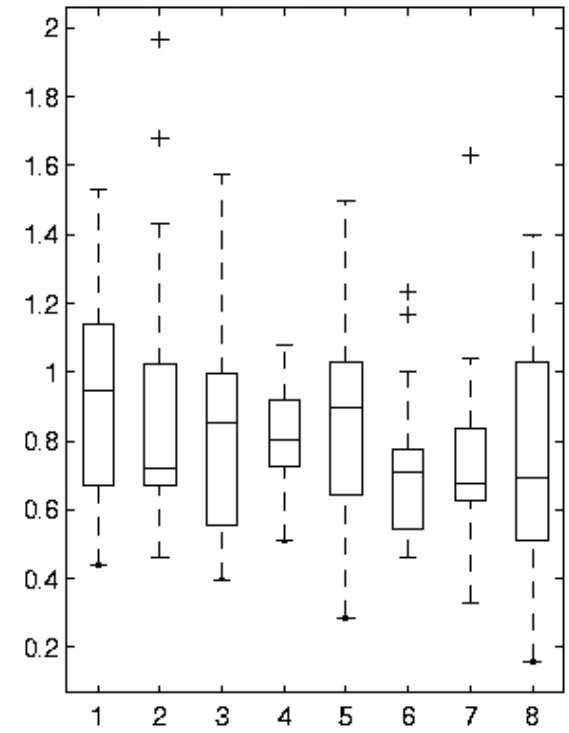
2
1.8
1.6
1.4
1.2
1
0.8
0.6
0.4
0.2
1 2 3 4 5 6 7 8

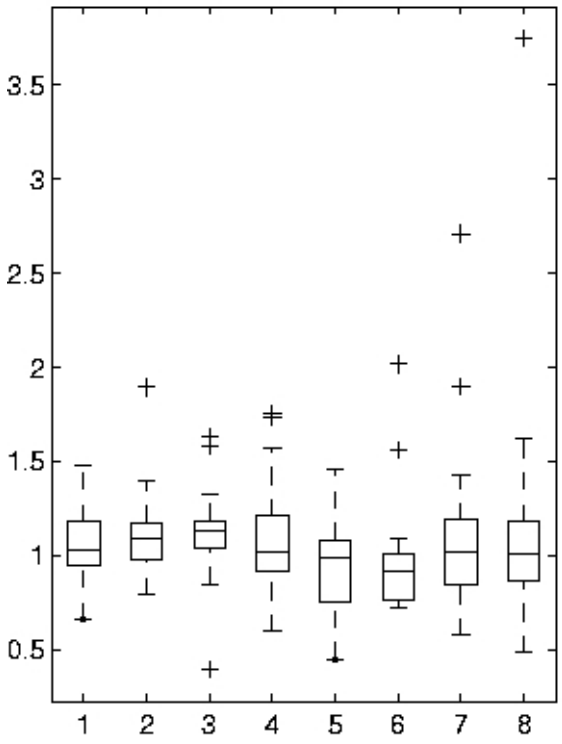
3.5
3
2.5
2
1.5
1
0.5
1 2 3 4 5 6 7 8

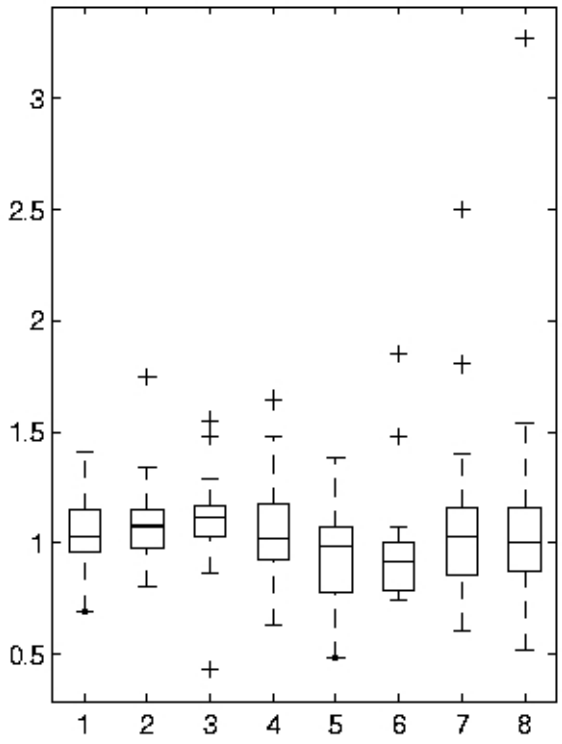
3
2.5
2
1.5
1
0.5
1 2 3 4 5 6 7 8

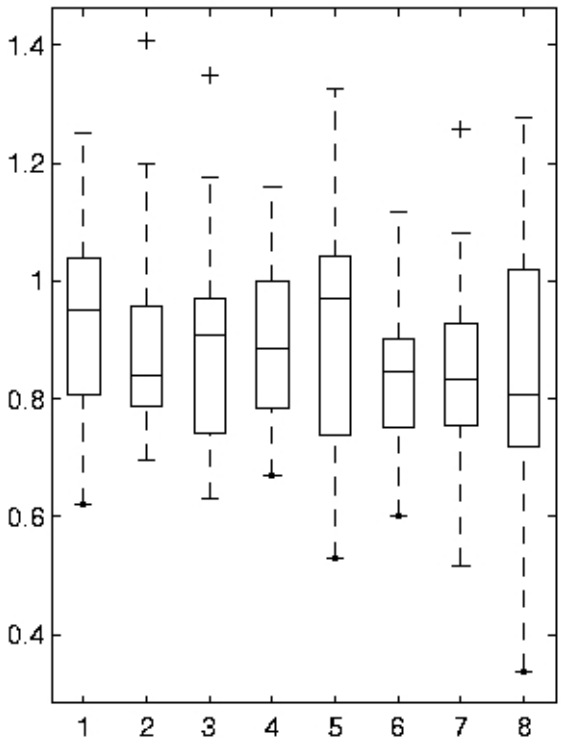
1.4
1.2
1
0.8
0.6
0.4
1 2 3 4 5 6 7 8

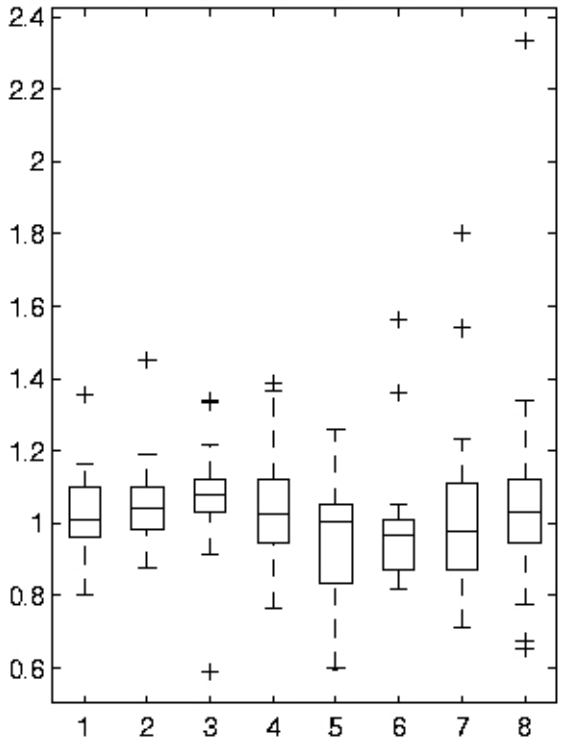
2.4
2.2
2
1.8
1.6
1.4
1.2
1
0.8
0.6
1 2 3 4 5 6 7 8

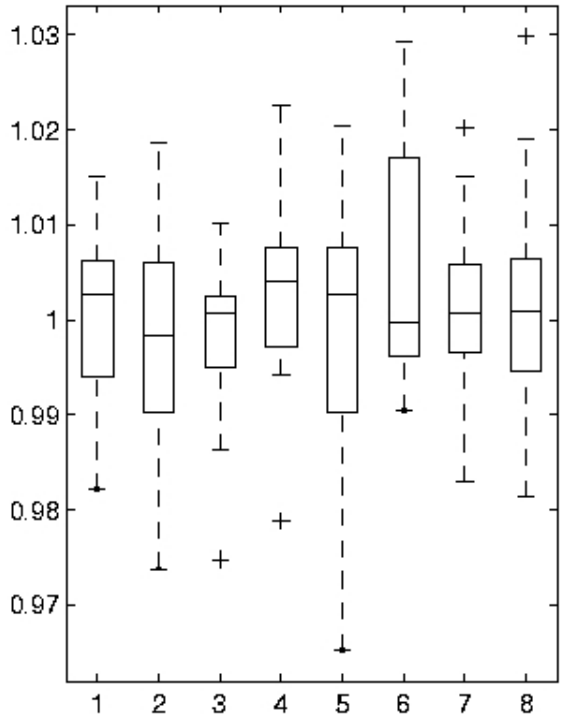
1.03
1.02
1.01
1
0.99
0.98
0.97
1 2 3 4 5 6 7 8

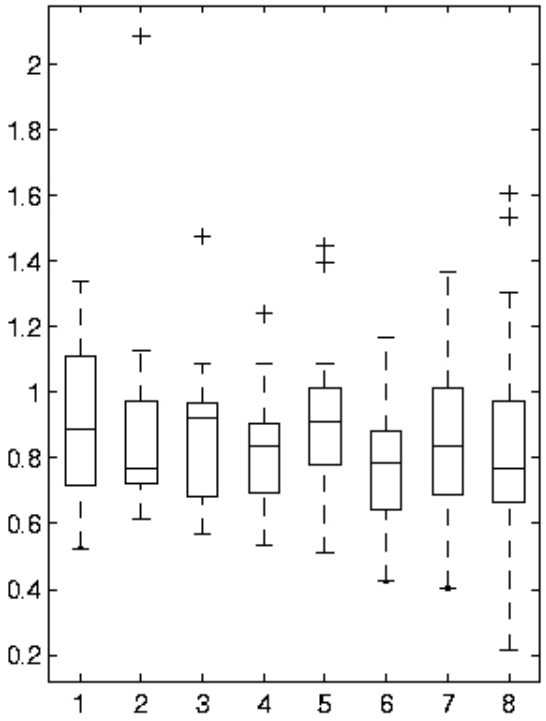
2
1.8
1.6
1.4
1.2
1
0.8
0.6
0.4
0.2
1 2 3 4 5 6 7 8

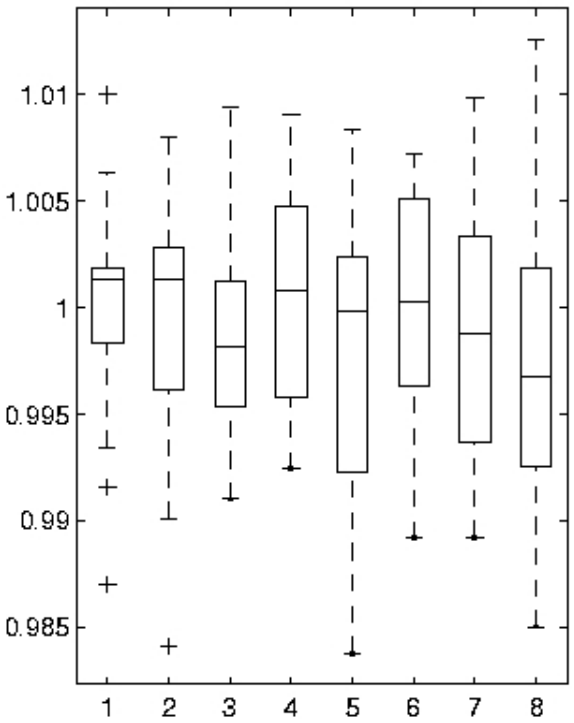
1.01
1.005
1
0.995
0.99
0.985
1 2 3 4 5 6 7 8

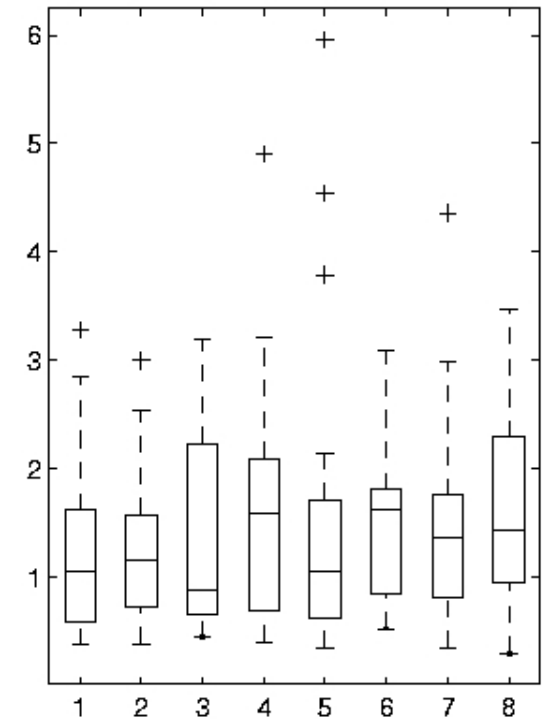
6
5
4
3
2
1
1 2 3 4 5 6 7 8

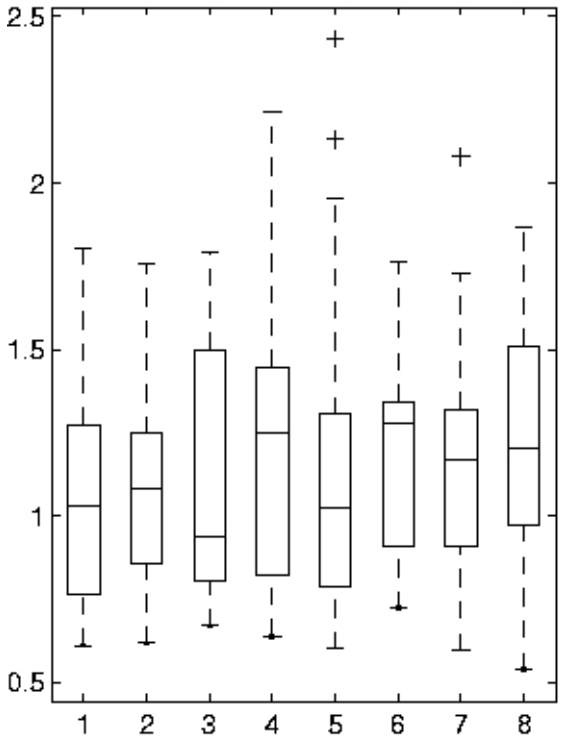
2.5
2
1.5
1
0.5
1
2
3
4
5
6
7
8

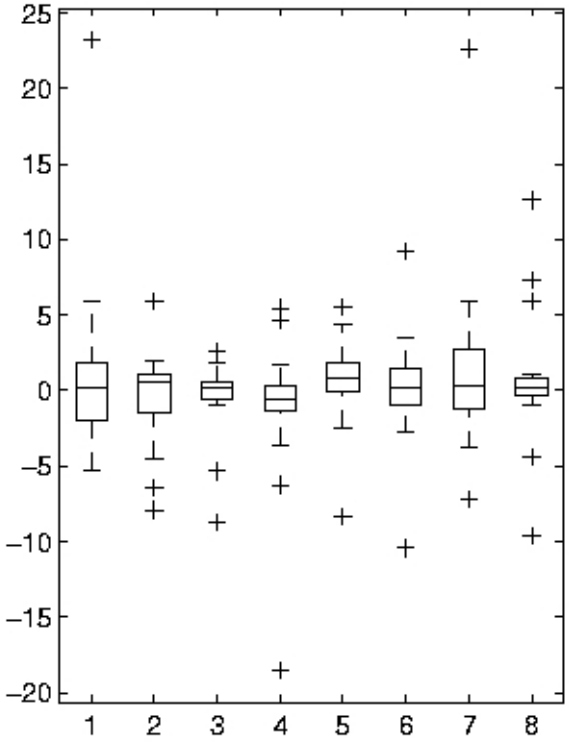
25
20
15
10
5
0
−5
−10
−15
−20
1
2
3
4
5
6
7
8

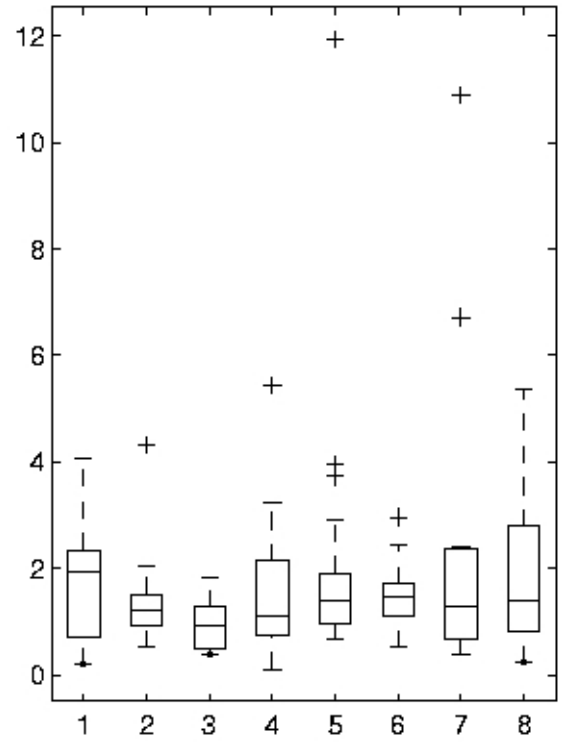
12
10
8
6
4
2
0
1
2
3
4
5
6
7
8

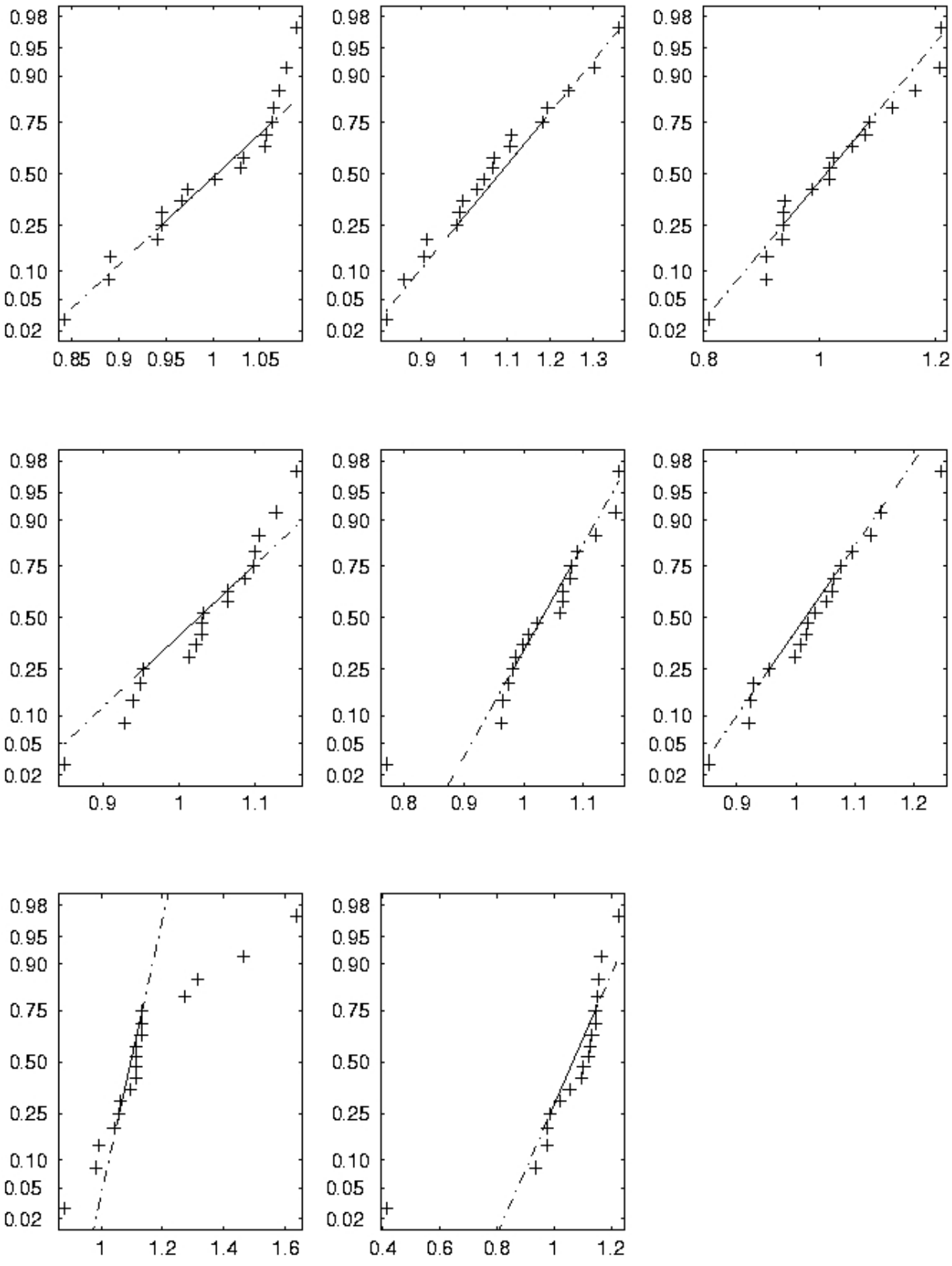
0.98
0.95
0.90
0.75
0.50
0.25
0.10
0.05
0.02
0.85 0.9 0.95 1 1.05
0.9 1 1.1 1.2 1.3
0.8 1 1.2
0.9 1 1.1
0.8 0.9 1 1.1
0.9 1 1.1 1.2
1 1.2 1.4 1.6
0.4 0.6 0.8 1 1.2

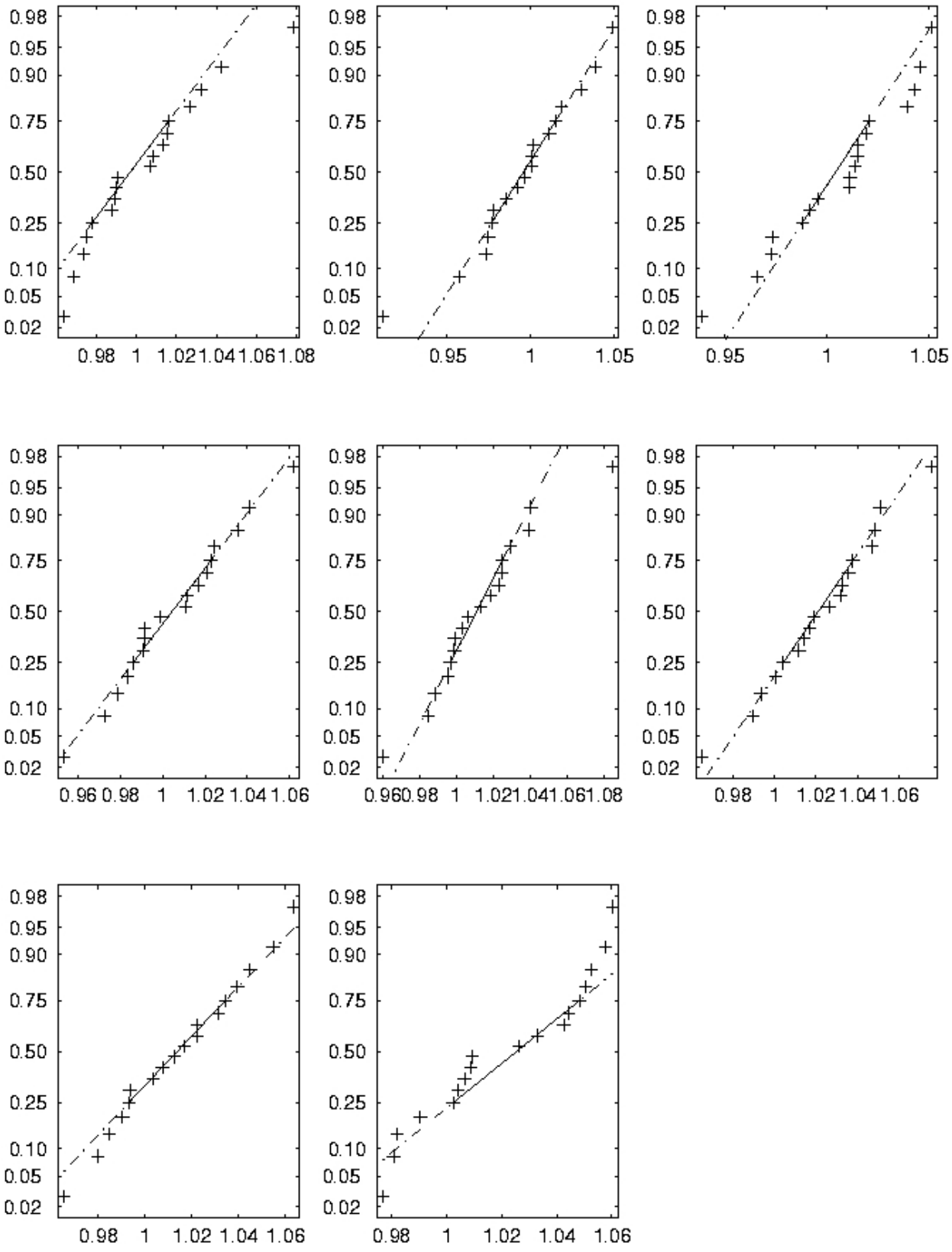
0.98
0.95
0.90
0.75
0.50
0.25
0.10
0.05
0.02
0.98 1 1.02 1.04 1.06 1.08
0.95 1 1.05
0.95 1 1.05
0.96 0.98 1 1.02 1.04 1.06
0.96 0.98 1 1.02 1.04 1.06 1.08
0.98 1 1.02 1.04 1.06
0.98 1 1.02 1.04 1.06
0.98 1 1.02 1.04 1.06

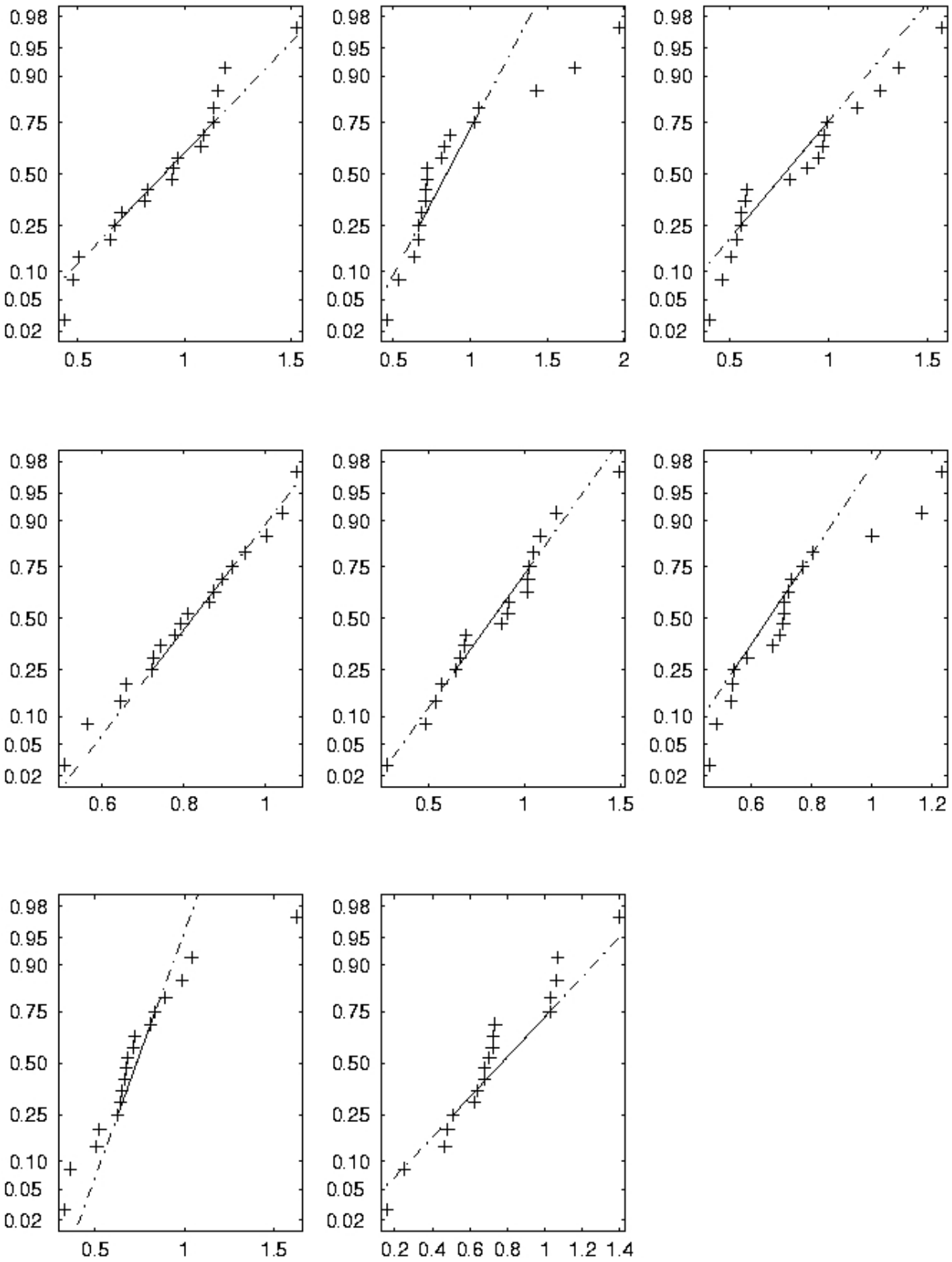
0.98
0.95
0.90
0.75
0.50
0.25
0.10
0.05
0.02
0.5
1
1.5
2
0.6
0.8
1.2
1.4
0.2
0.4

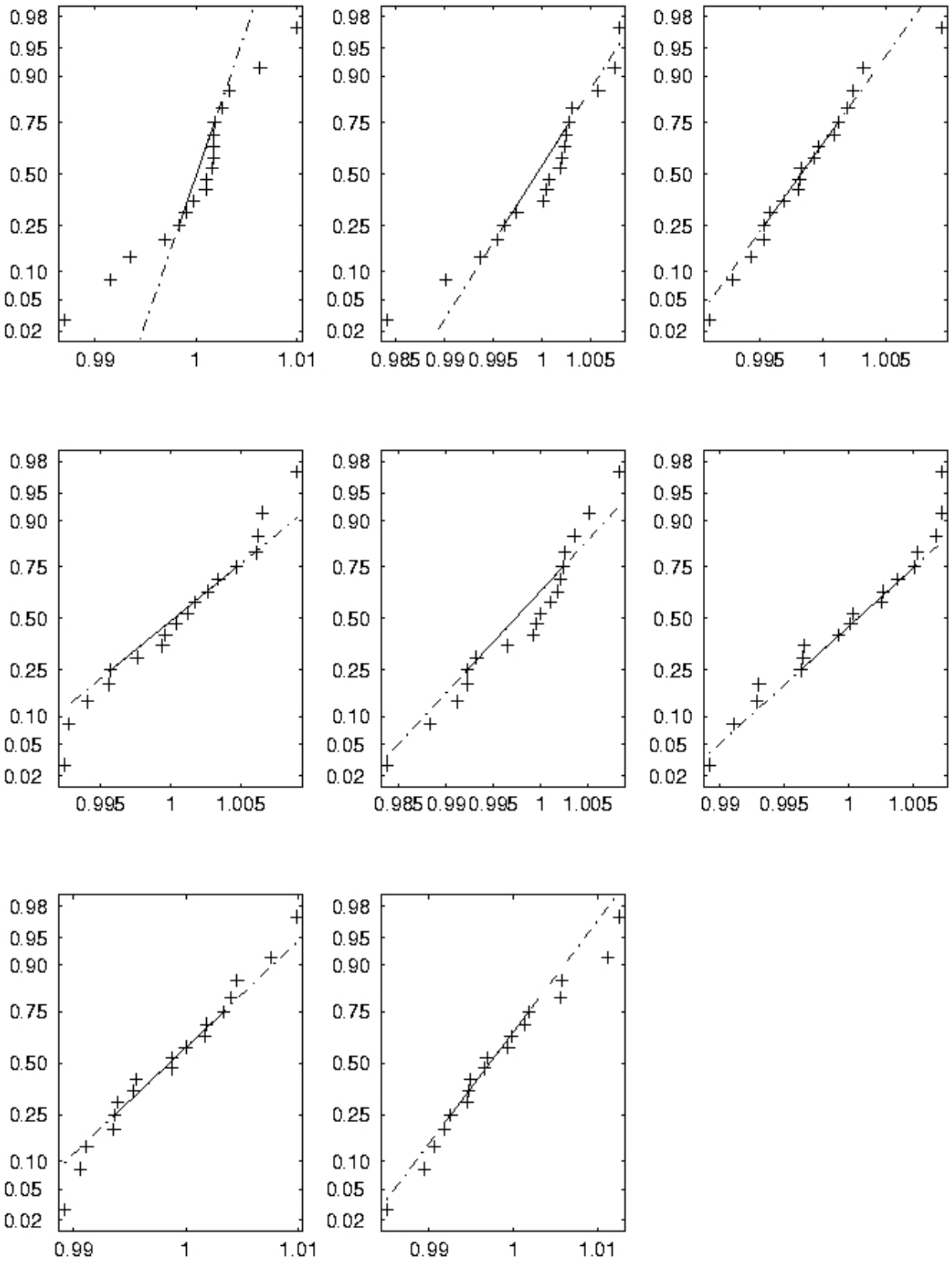
0.98
0.95
0.90
0.75
0.50
0.25
0.10
0.05
0.02
0.99
1
1.01
0.985
0.995
1.005

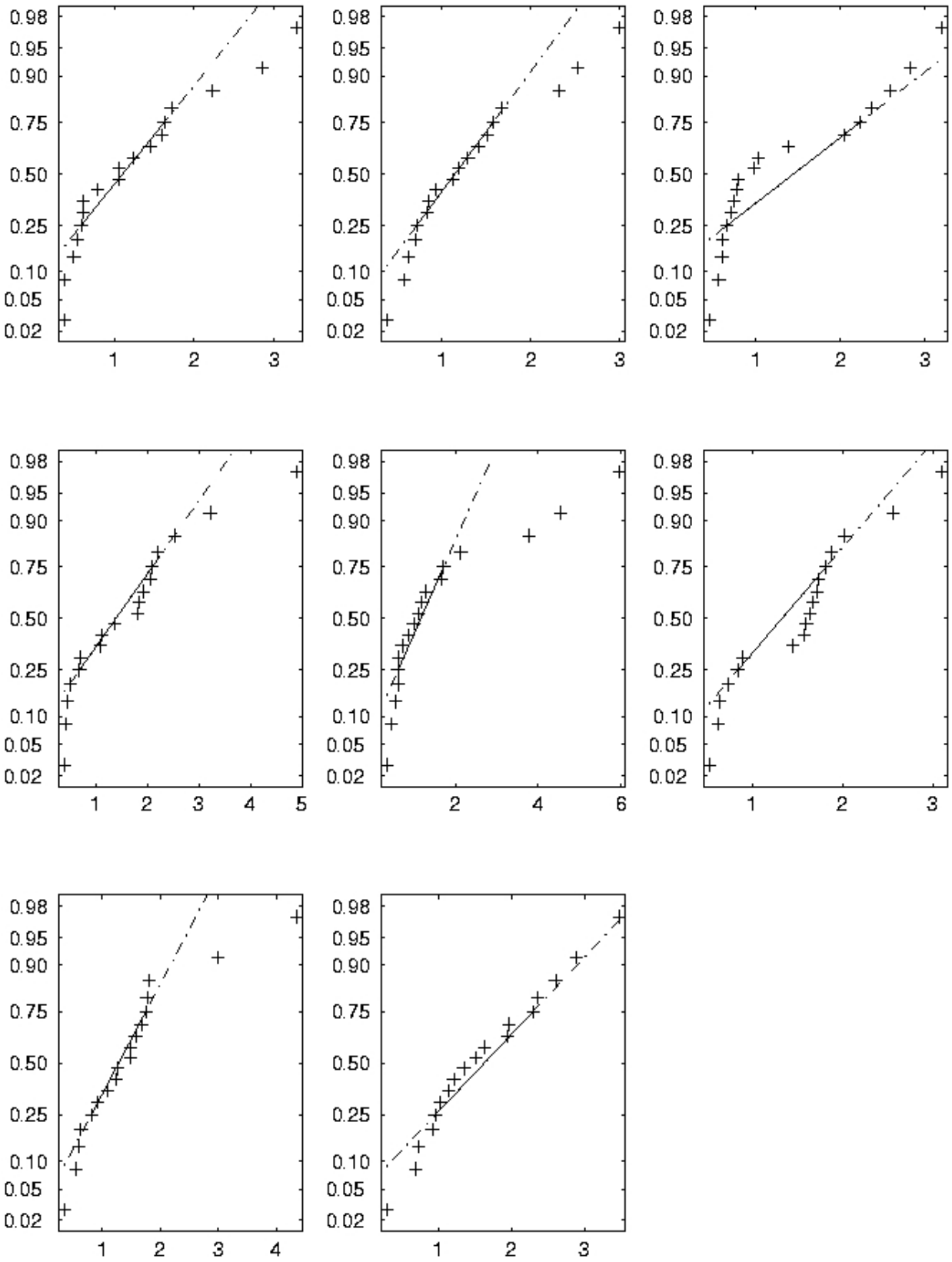
0.98
0.95
0.90
0.75
0.50
0.25
0.10
0.05
0.02
1
2
3
4
5
6

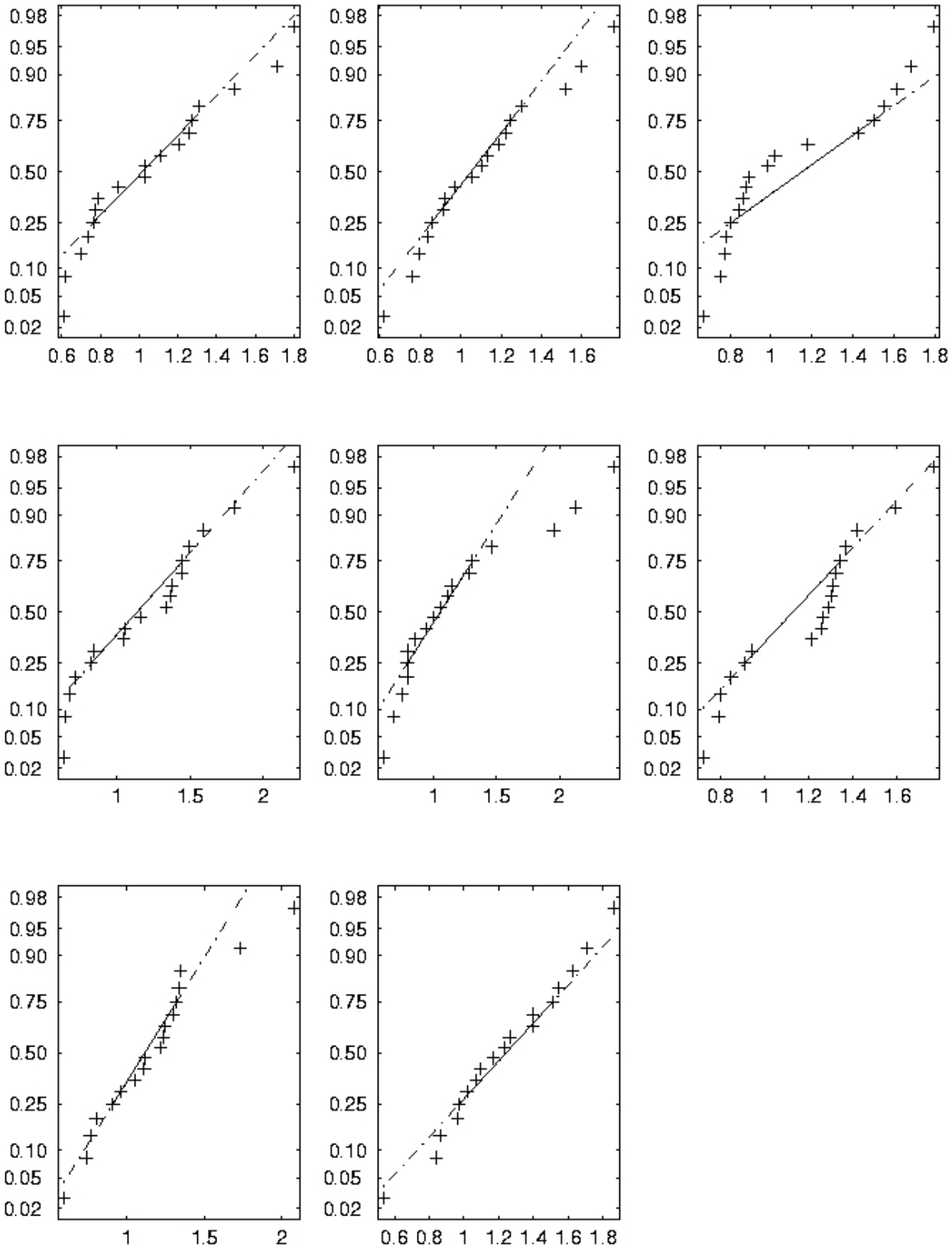
0.98
0.95
0.90
0.75
0.50
0.25
0.10
0.05
0.02
0.6 0.8 1 1.2 1.4 1.6 1.8
0.6 0.8 1 1.2 1.4 1.6
0.8 1 1.2 1.4 1.6 1.8
1 1.5 2
0.8 1 1.2 1.4 1.6
0.6 0.8 1 1.2 1.4 1.6 1.8